Photonics-based real-time and high-resolution ISAR imaging of non-cooperative target

Fangzheng Zhang (张方正), Qingshui Guo (郭清水), Ying Zhang (张 营), Yao Yao (姚 瑶), Pei Zhou (周 沛), Daiyin Zhu (朱岱寅), and Shilong Pan (潘时龙)*

Key Laboratory of Radar Imaging and Microwave Photonics, Ministry of Education, Nanjing University of Aeronautics and Astronautics, Nanjing 210016, China

**Corresponding author: pans@ieee.org*

Received July 6, 2017; accepted September 22, 2017; posted online October 19, 2017

Real-time and high-resolution imaging is demonstrated based on field trial detection of a non-cooperative target using a photonics-based inverse synthetic aperture radar (ISAR). By photonic generation and de-chirping of broadband linear frequency modulation signals, the radar can achieve a high range resolution thanks to the large instantaneous bandwidth (8 GHz at the K band), as well as real-time ISAR imaging using low-speed analog-to-digital conversion (25 MSa/s). A small-size unmanned aerial vehicle is employed as the non-cooperative target, and ISAR imaging is realized with a resolution far better than those achieved by the previously reported photonics-based ISARs. The capability for real-time ISAR imaging is also verified with an imaging frame rate of 25 fps. These results validate that the photonics-based radar is feasible in practical real-time and high-resolution ISAR imaging applications.

OCIS codes: 280.6730, 060.5625.
doi: 10.3788/COL201715.112801.

Inverse synthetic aperture radar (ISAR) imaging, which is implemented based on an advanced signal processing algorithm rather than large aperture antennas, is a promising technique to identify moving targets[1]. In applications such as pilotless automobiles, unmanned aerial vehicles (UAVs), and quick security checks, real-time ISAR imaging with a high-resolution is highly desired[2–4]. To achieve this goal, the ISAR should first emit a microwave signal with a large instantaneous bandwidth and then process the received echoes rapidly in the receiver[5]. However, direct generation of a linear frequency modulation (LFM) signal, a waveform that is commonly used in high-resolution ISARs, by means of a direct digital synthesizer (DDS) is limited to a few gigahertz (GHz)[6], so high imaging resolution is difficult to be achieved using conventional electronic technologies. To break the instantaneous bandwidth limitation, one method is to apply a high carrier frequency in the ISAR system. For example, a terahertz ISAR with a carrier frequency of 321 GHz and an instantaneous bandwidth of 10 GHz was reported, where a range resolution of ~1.5 cm was achieved[7]. However, the required multiple stages of frequency conversion, filtering, and amplification greatly increased the system complexity and severely deteriorated the signal quality and imaging performance. In addition, the detection range is limited for radars operated at the terahertz band because of small emission power and large atmospheric absorption, especially in extreme weather conditions. On the other hand, to achieve fast or even real-time ISAR imaging, de-chirping was applied in the receiver[8], but this technique still suffers from bandwidth and performance limitations of electronic signal processing, especially when a very large instantaneous bandwidth is adopted.

Microwave photonic technologies have been proposed for generating and processing high-frequency and broadband radio frequency (RF) signals[9–12], which provide solutions to overcome the bandwidth limitations in modern radars. For example, photonic generation of LFM signals with a bandwidth over 10 GHz can be easily implemented[13,14], and microwave photonic frequency converters can be operated with a frequency range of tens of GHz[15,16]. The great potential of microwave photonic technologies in future radar applications has been proved in a photonics-based fully digital coherent radar[17]. However, the signal bandwidth is only tens of megahertz (MHz), and the signal processing in the sampling receiver still restricts the operation bandwidth. To take full advantage of microwave photonic technologies in broadband radars, we have proposed a photonics-based ISAR, which has the ability for real-time and ultra-high-resolution imaging[18]. In this system, the broadband LFM signal is generated by photonic frequency quadrupling, and the received radar echo is de-chirped to a low-frequency signal based on photonic frequency mixing. Thanks to the large operation bandwidth of the photonic signal generation and de-chirp processing, a high range resolution can be achieved. Besides, sampling and processing of the low-frequency signal after de-chirping makes it feasible for the radar receivers to implement fast or even real-time ISAR imaging, which is verified through a turntable imaging experiment. However, in realistic scenarios, the targets to be detected are usually non-cooperative, i.e. the distance, speed, and moving direction are unknown. Thus, ISAR imaging of non-cooperative targets is necessary[19,20]. Evaluation of the performance of non-cooperative-target ISAR imaging is of great importance for practical applications of the photonics-based ISAR.

In this Letter, we demonstrate and investigate ISAR imaging based on the field trial detection of a non-cooperative target using a photonics-based radar with an 8 GHz bandwidth in the K band (18–26 GHz). High-resolution ISAR imaging of a flying UAV with a size of less than 2 m is carried out. The imaging resolution is far better than those achieved by previously reported photonics-based radars. Besides, fast ISAR imaging with a frame rate as high as 25 fps is demonstrated, confirming the capability of the photonics-based radar for real-time ISAR imaging with a recorded high resolution.

Figure 1 shows the schematic diagram of the photonics-based ISAR[18]. A continuous-wave (CW) light from a laser diode (LD) is modulated by a dual-parallel Mach–Zehnder modulator (DPMZM), which is driven by an intermediate frequency (IF) band LFM CW (LFMCW) signal generated by a low-speed electrical signal generator. The IF-LFMCW signal passes through an electrical 90° hybrid coupler. The two output signals are applied to the two RF ports of the DPMZM. After properly setting the bias voltages, the DPMZM works at the frequency quadrupling mode[21], i.e., only the ±2nd-order modulation sidebands are generated. Then, the optical signal is equally split into two branches by an optical coupler (OC). The signal in the lower branch is used as a reference for de-chirping the radar echoes. In the upper branch, the optical signal is sent to a photodetector (PD1) to perform optical-to-electrical conversion. After PD1, an LFMCW signal is generated, of which the frequency and bandwidth are quadrupled, as compared with the original IF-LFMCW signal[22]. The generated LFMCW signal is amplified by an electrical amplifier (EA1) before emitting to the free space through a transmit antenna (Tx) for ISAR imaging. The echoes reflected from the targets are collected by a receive antenna (Rx) and properly amplified by EA2 before being applied to an electro-optical phase modulator (PM) to modulate the reference optical signal, which can be treated as two frequency-sweeping optical carriers. After the PM, at a given time, the first-order sideband generated by phase modulation of the first optical carrier would be located closely to the second optical carrier in the spectrum. Then, an optical bandpass filter (OBPF) is used to select out this first-order phase modulation sideband and the second optical carrier. The obtained optical signal is sent to PD2 to perform photonic frequency mixing. After PD2, an electrical low-pass filter (ELPF) with a proper bandwidth is used to remove the high-frequency interference. To this point, de-chirping of the received LFM signal is completed[18]. The de-chirped signal after the ELPF has a frequency of $\Delta f = k\Delta\tau$, where k is the chirp rate of the transmitted LFMCW signal, and $\Delta\tau$ is the time delay of the echo signal compared with the transmitted LFMCW signal. By properly setting the chirp rate of the transmitted LFMCW signal according to the detection range, the signal after de-chirping can be controlled to a low frequency, and it can be digitalized by a low-speed analog-to-digital converter (ADC) with a high precision. The digitized signal can be processed in a digital signal processing (DSP) unit based on mature ISAR imaging algorithms. Theoretically, the range resolution of the ISAR is[1]

$$L_{\mathrm{RES}} = \frac{c}{2B}, \tag{1}$$

where B is the bandwidth of the LFMCW signal, and the cross-range resolution is given by[1]

$$C_{\mathrm{RES}} = \frac{c}{2\theta f_c}, \tag{2}$$

where f_c is the center frequency of the LFMCW signal, and θ is the total viewing angle of target rotating. Thanks to the use of photonic frequency quadrupling and photonic de-chirping, the photonics-based ISAR has the potential to be operated at a bandwidth as large as tens of even hundreds of GHz. Thus, an ultra-high range resolution below 1 cm is realizable. In the receiver, only a low-frequency signal is needed to be sampled and processed, making the system competent for real-time ISAR imaging with the existing digital radar receivers.

Figure 2(a) shows the picture of the radar system used for field trial ISAR imaging. An electrical arbitrary waveform generator (AWG, Keysight 8195A) with a sampling rate of 65 GSa/s is applied to generate an IF-LFMCW signal, which has a repetition rate of 5 kHz and a bandwidth of 2 GHz (4.5–6.5 GHz). An LD (TeraXion Inc., 1550.12 nm), a DPMZM (Fujitsu FTM7962EP), the PM (EOSAPCE Inc.), an OBPF (Yenista XTM-50), one 40 GHz PD (u2t XPDV2120RA), one 10 GHz PD (CONQUER Inc.), and two EAs (SHF 806E, 26 dB gain) are placed inside the photonic box, where the photonic frequency quadrupling and de-chirping are performed, as shown in Fig. 2(a). At the output of the photonic box, the generated LFMCW signal has a bandwidth of 8 GHz (18–26 GHz). The LFMCW signal from the photonic box is further amplified by a high-power amplifier (HPA, Agilent 83020A, bandwidth 2–26.5 GHz). After the HPA, the signal with a power of about 23 dBm is directed to a Tx. The received echo is collected by a Rx, which is placed about 20 cm apart from the Tx. The two antennas are both horn antennas operated at

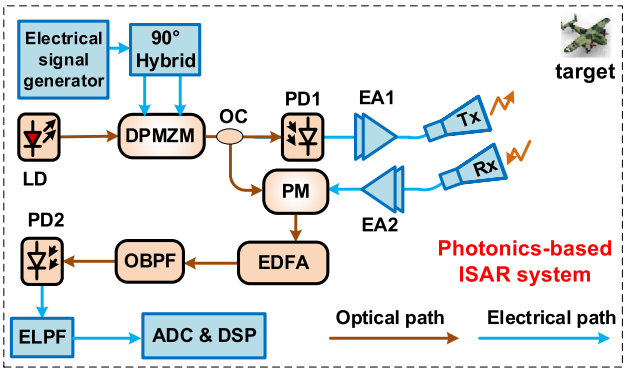

Fig. 1. Schematic diagram of the photonics-based ISAR system.

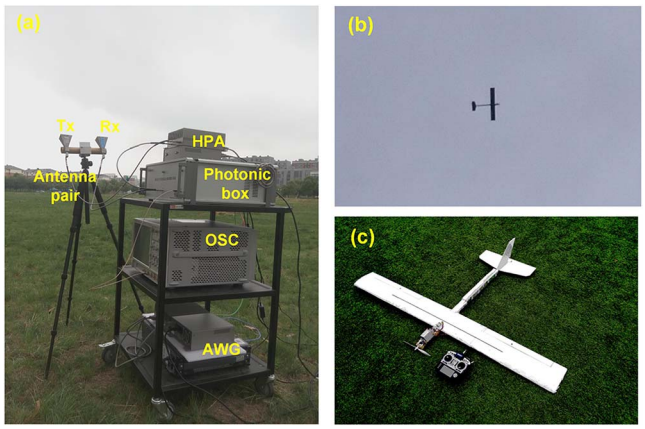

Fig. 2. (a) Picture of the radar system for field trial ISAR imaging experiment, (b) picture of the flying UAV, and (c) picture of the UAV placed on the ground.

the K band, and both have an elevation of about 60° toward a UAV, which is remotely controlled to fly in the horizontal direction. Figure 2(b) is a picture of the flying UAV captured by a camera. The picture in Fig. 2(c) shows the static UAV, which has a much smaller size than the targets used in previous ISAR imaging working in the K band. Specifically, the length and width of the UAV's wing are 180 and 20 cm, respectively, and the length of the fuselage is 150 cm. The signal after de-chirping in a duration of 200 ms is sampled and recorded by a real-time oscilloscope (OSC, Keysight DSO-X 92504A) working at a sampling rate of 25 MSa/s. This sampling rate is sufficient, since the signal after de-chirping is located at around 4.5 MHz. When reconstructing the ISAR image, the coherent integration time, corresponding to an imaging frame, is set to 40 ms. Thus, each imaging frame has 200 radar pulses, and the Doppler frequency resolution is 25 Hz. Based on the recorded data, ISAR imaging is implemented by windowed two-dimensional Fourier transformation, i.e., a fast Fourier transform (FFT) is first performed on the samples to reconstruct the high-resolution range profiles, and then an FFT is applied to each range bin to obtain the cross-range dimensions.

Figure 3(a) shows the recovered range profile of the UAV as a function of time in one frame. As can be seen, the target appears at a distance of about 17 m. Figure 3(b) shows the reconstructed ISAR image, which has a maximum Doppler shift of ~400 Hz. According to Eq. (1), the range resolution of the established ISAR is 1.875 cm. Since the radar resolution is much smaller than the size of the UAV, clear images in both the range and cross-range profiles are achieved in Fig. 3(b). In previous field trial demonstrations of photonics-based ISAR imaging, the operation bandwidth is 125[23] and 600 MHz[24], corresponding to a range resolution of 1.2 m and 25 cm, respectively. Therefore, the imaging resolution in this demonstration is far better than that achieved by previously reported photonics-based radars.

In the existing digital ISAR receivers, real-time signal processing at a sampling rate of 25 MSa/s is not a problem. To verify the real-time imaging capability, ISAR images in four successive frames are reconstructed based on the data with a duration of 160 ms with the results shown in Fig. 4. As can be seen from the images, the UAV flies at the same height of about 17 m. By comparing the Doppler shifts in the cross-range, the moving property of the UAV can be confirmed. In this demonstration, the frame rate of ISAR imaging reaches as high as 25 fps, indicating that a near real-time ISAR imaging can be achieved with very high resolution.

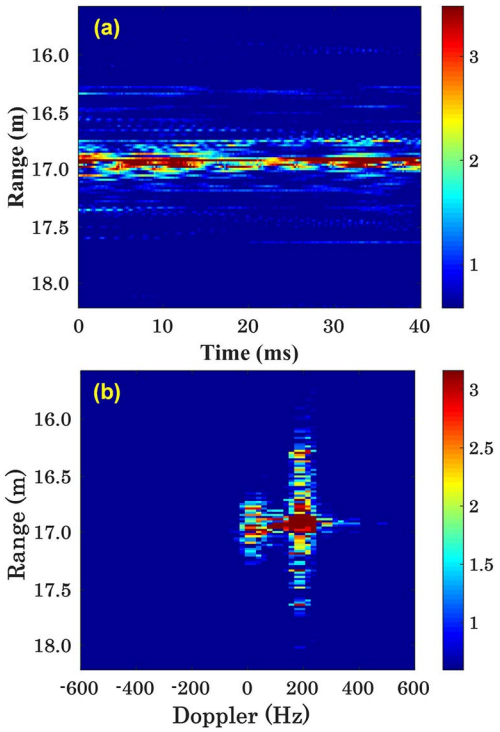

Fig. 3. (a) Recovered range profile of the UAV as a function of time in a frame of 40 ms, and (b) the reconstructed ISAR image of the UAV in the same frame.

In conclusion, we demonstrate and evaluate the performance of the field trial of a photonics-based ISAR for

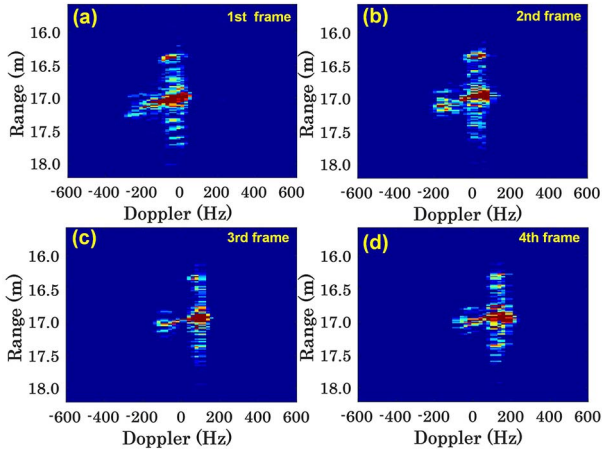

Fig. 4. ISAR imaging results in the first, second, third, and fourth frames.

real-time and high-resolution imaging. High-resolution ISAR images of a small-size UAV are achieved, and fast ISAR imaging at 25 fps is demonstrated. The results can confirm that the photonics-based ISAR is competent for practical applications, where real-time and high-resolution imaging is required.

This work was supported in part by the National Natural Science Foundation of China (Nos. 61401201 and 61422108), the Aviation Science Foundation of China (No. 2015ZC52024), and the Open Fund of Science and Technology on Monolithic Integrated Circuits and Modules Laboratory (No. 20150C1404).

References

1. V. C. Chen and M. Martorella, *Inverse Synthetic Aperture Radar Imaging: Principles, Algorithms and Applications* (SciTech Publishing, 2014).
2. P. Almorox-Gonzalez, J. T. González-Partida, M. Burgos-García, C. D. L. Morena-Alvarez-Palencia, L. Arche-Andradas, and B. P. Dorta-Naranjo, in *Proceedings of 2007 International Conference Sensor Technologies Applications* (2007).
3. B. Valdes, Y. Alvarze, S. Mantzavinos, F. Las-Heras, and J. A. Martinez-Lorenzo, IEEE Antennas Propag. Mag. **58**, 35 (2016).
4. J. Ping, A. Ling, T. Quan, and C. Dat, in *IEEE Proceedings of Conference on Sustainable Utilization and Development in Engineering and Technology* (2012), p. 289.
5. D. A. Robertson, D. G. Macfarlane, R. I. Hunter, C. L. Cassidy, N. Liombart, E. Candini, T. Bryllert, M. Ferndahl, H. Lindstrom, J. Tenhunen, H. Vasama, J. Huopana, T. Selkala, and A. J. Vuotikka, Proc. SPIE **10189**, 101890C (2017).
6. Q. Li, D. Yang, X. H. Mu, and Q. L. Huo, in *International Conference on Microwave and Millimeter Wave Technology (ICMMT)* (2012).
7. Q. Yang, B. Deng, H. Wang, and Y. Qing, Electron. Lett. **52**, 2059 (2016).
8. B. B. Cheng, G. Jing, C. Wang, C. Yang, Y. W. Cai, Q. Chen, X. Huang, G. H. Zeng, J. Jiang, X. J. Deng, and J. Zhang, IEEE Trans. THz Sci. Technol. **3**, 606 (2013).
9. J. Capmany and D. Novak, Nat. Photon. **1**, 319 (2007).
10. J. Yao, IEEE J. Lightwave Technol. **27**, 314 (2009).
11. W. Zhai, X. Gao, W. Xu, M. Zhao, M. Xie, S. Huang, and W. Gu, Chin. Opt. Lett. **14**, 040601 (2016).
12. X. Ye, B. Zhang, Y. Zhang, D. Zhu, and S. Pan, Chin. Opt. Lett. **15**, 010013 (2017).
13. P. Zhou, F. Zhang, Q. Guo, and S. Pan, Opt. Express **24**, 18460 (2016).
14. H. Zhang, W. Zou, and J. Chen, Opt. Lett. **40**, 1085 (2015).
15. E. H. W. Chan and R. A. Minasian, J. Lightwave Technol. **30**, 3580 (2012).
16. Z. Z. Tang and S. L. Pan, IEEE Trans. Microwave Theory Tech. **64**, 3017 (2016).
17. P. Ghelfi, F. Laghezza, F. Scotti, G. Serafino, A. Capria, S. Pinna, D. Onori, C. Porzi, M. Scaffardi, A. Malacarne, V. Vercesi, E. Lazzeri, F. Berizzi, and A. Bogoni, Nature **507**, 341 (2014).
18. F. Zhang, Q. Guo, Z. Wang, P. Zhou, G. Zhang, J. Sun, and S. Pan, Opt. Express **25**, 16274 (2017).
19. J. Zheng, T. Su, L. Zhang, W. Zhu, and Q. H. Liu, IEEE Trans. Geosci. Remote Sens. **52**, 7276 (2014).
20. J. Zheng, T. Su, W. Zhu, and Q. H. Liu, IEEE Trans. Geosci. Remote Sens. **11**, 1275 (2014).
21. C. Lin, P. Shih, J. Chen, W. Xue, P. Peng, and S. Chi, IEEE Photon. Technol. Lett. **20**, 1027 (2008).
22. Q. Guo, F. Zhang, P. Zhou, and S. L. Pan, IEEE Photon. Technol. Lett. **29**, 1320 (2017).
23. F. Laghezza, F. Scotti, D. Onori, and A. Bogoni, in *The 17th International Radar Symposium (IRS)* (2016).
24. R. Li, W. Li, M. Ding, Z. Wen, Y. Li, L. Zhou, S. Yu, T. Xing, B. Gao, Y. Luan, Y. Zhu, P. Guo, Y. Tian, and X. Liang, Opt. Express **25**, 14334 (2017).